











RESEARCH ARTICLE

Nanoscale hybrid implant surfaces and *Osterix*-mediated osseointegration

Laís Morandini Rodrigues¹  | Elis A. Lima Zutin¹  | Elisa M. Sartori²  |
Fabio A. P. Rizzante³  | Daniela B. S. Mendonça⁴  | Paul H. Krebsbach⁵  |
Karl J. Jepsen⁶  | Lyndon F. Cooper⁷  | Luana M. R. Vasconcelos¹  |
Gustavo Mendonça⁴ 

¹Department of Biosciences and Oral Diagnosis, Institute of Science and Technology, São Paulo State University (Unesp), São José dos Campos, Brazil

²Department of Oral Surgery and Integrated Clinics, School of Dentistry, São Paulo State University (Unesp), Araçatuba, Brazil

³Department of Comprehensive Dentistry, School of Dental Medicine, Case Western Reserve University, Cleveland, Ohio, USA

⁴Department of Biological and Material Sciences & Prosthodontics, School of Dentistry, University of Michigan, Ann Arbor, Michigan, USA

⁵Section of Periodontics, School of Dentistry, University of California, Los Angeles, California, USA

⁶Department of Orthopedic Surgery, School of Medicine, University of Michigan, Ann Arbor, Michigan, USA

⁷Department of Oral Biology, College of Dentistry, University of Illinois at Chicago, Chicago, Illinois, USA

Correspondence

Gustavo Mendonça, Biologic and Materials Sciences & Prosthodontics, 1011 N University Ave, Rm 3165, Ann Arbor, MI 48109-1078, USA.
Email: mgustavo@umich.edu

Funding information

Academy of Osseointegration; International Association for Dental Research; National Institute of Arthritis and Musculoskeletal and Skin Diseases, Grant/Award Number: P30 AR069620

Abstract

Endosseous implant surface topography directly affects adherent cell responses following implantation. The aim of this study was to examine the impact of nanoscale topographic modification of titanium implants on *Osterix* gene expression since this gene has been reported as key factor for bone formation. Titanium implants with smooth and nanoscale topographies were implanted in the femurs of *Osterix*-Cherry mice for 1–21 days. Implant integration was evaluated using scanning electron microscopy (SEM) to evaluate cell adhesion on implant surfaces, histology, and nanotomography (NanoCT) to observe and quantify the formed bone-to-implant interface, flow cytometry to quantify of *Osterix* expressing cells in adjacent tissues, and real-time PCR (qPCR) to quantify the osteoinductive and osteogenic gene expression of the implant-adherent cells. SEM revealed topography-dependent adhesion of cells at early timepoints. NanoCT demonstrated greater bone formation at nanoscale implants and interfacial osteogenesis was confirmed histologically at 7 and 14 days for both smooth and nanosurface implants. Flow cytometry revealed greater numbers of *Osterix* positive cells in femurs implanted with nanoscale versus smooth implants. Compared to smooth surface implants, nanoscale surface adherent cells expressed higher levels of *Osterix* (*Osx*), Alkaline phosphatase (*Alp*), Paired related homeobox (*Prx1*), Dentin matrix protein 1 (*Dmp1*), Bone sialoprotein (*Bsp*), and Osteocalcin (*Ocn*). In conclusion, nanoscale surface implants demonstrated greater bone formation associated with higher levels of *Osterix* expression over the 21-day healing period with direct evidence of surface-associated gene regulation involving a nanoscale-mediated osteoinductive pathway that utilizes *Osterix* to direct adherent cell osteoinduction.

KEYWORDS

bone-implant interface, gene expression, nanostructured materials, osseointegration, surface topography

1 | INTRODUCTION

Many studies have targeted the implant surface to improve osseointegration.^{1,2} The implant surface influences adhesion, proliferation and cellular differentiation to promote bone formation.¹⁻⁵ Bone structure from the macro to the nanostructure^{4,6} inspires the engineering of endosseous implant surfaces and surfaces that mimic the hierarchical characteristics of bone at the micron- and the nano-scale levels.^{4,5} Implant surfaces with nanostructures of 1–100 nm enhance osteoblast maturation,^{7,8} increase bone-to-implant contact (BIC),⁹ and improve clinical success rates.¹⁰ Many methods alter surface topography that enhances the osseointegration process at titanium dental implants.¹¹ Among these, grit blasting in combination with acid etching and peroxidation can modify Ti surface topography to produce hierarchical micron- and nano-scale topographic features.

This superimposition of nano features on micro scale topographies increases osteogenesis at implant surfaces,^{1,8,12,13} and influences the differentiation of mesenchymal stem cells into osteoblasts.^{8,14} The role of the multi-scale micro- and nanoscale surfaces on osseointegration has been investigated in a systematic way in vivo.¹¹ Importantly, the understanding of the molecular and cellular mechanisms underlying cellular and tissue interaction with nanoscale topography in vivo remains incomplete.

Endosseous dental implants are placed through the cortex into the medullary bone marrow. A reservoir of skeletal stem cells/progenitors, immune cells and relatively undifferentiated osteoprogenitor cells (mesenchymal stem cells) that direct osteogenesis are present in this location.^{15,16} In cell culture,⁸ in rodent models^{17,18} and in humans,^{19,20} implant topography alters implant adherent cell osteoinductive gene expression at the level of *Runx2* and *Osterix*. The greater fold induction for *Osterix* compared to *Runx2* expression in cells adherent to hybrid nano/micro versus micro topography surfaces implicates nanoscale features of the surface in signaling of osseointegration through and *Osterix*-dependent pathway.^{8,12,21}

Here, we deployed the *Osterix*-Cherry reporter mouse model to directly evaluate the impact of nanoscale/micron surface topography on osteoinduction involving *Osterix* expression in vivo, once this gene is an osteoblast-specific transcription factor and induces the expression of mature osteoblast genes, being the subject of several studies directed to the process of osteointegration of implants. We had previously demonstrated the benefits of this nanoscale surface in vitro.⁸ In the *Osterix*-Cherry transgenic reporter mouse, direct and indirect reporting of *Osterix* expression demonstrated greater *Osterix* expression in nanoscale/micron topography implant adherent cells that was associated with (1) accelerated osteogenic gene expression and (2) increased BIC. In this study the *Osterix*-Cherry transgenic reporter mouse allowed to track *Osterix* protein expression in real-time with in forming bone at the implant interface.

2 | MATERIALS AND METHODS

2.1 | Sample preparation

Commercially pure grade IV titanium implants (8 mm × 0.9 mm) were prepared as previously described.⁸ Briefly, implants for the nanoscale group were grit blasted with 100- μ m aluminum oxide particles and sonicated three times in ultrapure deionized (DI) water (resistivity 1/4 8.2MO, pH 1/4 6.82; Millipore) for 15 min each followed by immersion in 1:1 vol/vol % solution of 30% H₂O₂ and 2N H₂SO₄ (Fisher Scientific, Pittsburgh, PA, United States) overnight. The implants were cleaned by sonication for 15 min three times in ultrapure deionized water, and then three times in 70% ethanol, before drying with ultraviolet (UV) light under a hood for 30 min. The implants prepared in this manner possess micron-scale surfaces with superimposed nanoscale topographic features and are hereafter referred to as “nano.” Samples that did not receive any surface treatment were cleaned following the same DI water and ethanol cleaning and sterilization by UV light are referred to as “smooth.”

2.2 | Mice surgery

All animal procedures were performed in accordance with a protocol approved by the Institutional Animal Care and Use Committee at the University of Michigan and in conformity with the ARRIVE guidelines. The Tg (Sp7/mCherry)2Pmay/J (OSX-Cherry) was obtained from Jackson Laboratory (Stock No: 024850 Bar Harbor, ME, United States) mouse contained one copy of the *Osterix* (SP7) gene tagged with a cherry fluorescent protein allowing visualization of osteoblast differentiation. OSX-cherry mice were bred with C57BL/6J (Stock No: 000664) to obtain heterozygous mice containing the OSX-cherry gene. Positive confirmation of an OSX-Cherry mouse phenotype was carried out by cutting a small piece of the tail (1–2 mm) at the time of weaning and observing red color of the bone using a fluorescence microscope. Forty-eight male mice (average body weight of 30 g and 7–8 weeks old) were used for surgery. The animals were housed in individual cages, with freely available water and food, and an artificial day/night cycle of 12 h/12 h in an air-conditioned room. The mice were anesthetized by isoflurane inhalation 2% and medicated before surgery with anti-inflammatory and analgesic drugs (5 mg/kg Carprofen[®]base, Pfizer) subcutaneously. The surgery region was shaved and disinfected with iodine solution (Betadine 10%, Meda). The incision was made in the medial parapatellar region with displacement and remoteness from the muscle complex, and the implants were placed in the long axis of the femur through a medial parapatellar arthrotomy, filling the entire medullary canal. A sequence of needles with 25, 23, and 20 gauges were used to perforate the proximal epiphysis and to access the intramedullary canal. The tissues were repositioned by means of a 5-0 Vicryl[®] suture (Ethicon, San Angelo, TX, United States). The animals were medicated with

anti-inflammatory and analgesic drugs (5 mg/kg Carprofen® base, Pfizer) subcutaneously for 48 h post-surgery and were kept in cages in groups of five. Euthanasia occurred at several time points post-surgery through the inhalation of carbon dioxide, and the segments of femurs with the implants were processed for the experiments.

2.3 | Surface analysis by scanning electron microscopy

The surfaces of the prepared implants were examined with a high-resolution scanning electron microscope (Philips XL30 FEG, SEM, Philips, Eindhoven, Netherlands). Observations were made at different magnifications aiming to show the differences between the smooth and nano-scale surfaces. Additional surface analyses were made of the implant surfaces removed from femurs 7 days following implantation. Atomic force microscopy (AFM; VEECO, MULTIMODE V, Digital Instruments, Santa Barbara, CA, United States) was used to demonstrate parameters of surface topography (*Ra*). Measurements at three randomly selected points were taken on the disk surfaces and average values were calculated.

2.4 | Wettability

Since the titanium implants placed on the femurs of the mice were too small to have their wettability calculated, the nanoscale surface was re-created on titanium discs measuring 20.0 mm × 1.0 mm (VULCANIUM Metals International, Northbrook, IL, United States). The samples were washed with acetone P.A. (Sigma-Aldrich®) using ultrasound for 5 min. Two drops of water in the amount of 0.5–0.75 µl were placed on the sample and the contact angle (CA) was obtained for each drop using a Drop Shape Analyzer 4500 (Kruss) goniometer. Measurements were made in a laboratory atmosphere with ~60% humidity. The equipment connected to the One Attension software was responsible for measuring CA through the sessile drop method. The chamber coupled to the goniometer made 50 shots per second and the formed CA was calculated.

2.5 | Histology

Euthanasia for histological examination was performed at days 7 and 14 after surgery (*n* = 5 animals). Muscle tissue and epiphyses were removed, and bones/implants were fixed with 4% paraformaldehyde (Z Fix) and decalcified with 10% EDTA (Sigma Aldrich) solution for 7 days at 4°C and under agitation. After decalcification, the implants were removed, and femurs were washed in MilliQ water. For the hematoxylin and eosin staining, the femurs were dehydrated in a graded series of ethanol concentrations and subsequently embedded in paraffin. Longitudinal cuts were made on the long axis of the femur to evaluate the BIC. Blocks were cut and ground to a final thickness of ~5 µm using a Leica RM2155 microtome (Leica, Wetzlar, Germany), available at University of Michigan, Histology Core.

2.6 | NanoCT

After 14 and 21 days, the mice were euthanized (*n* = 5 animals) and the femurs with implants were obtained for nanoCT analysis. The samples were fixed with paraformaldehyde (Z Fix) and non-destructive analysis of the newly formed bone at the implant interface was performed. The femurs containing the implants were imaged using a nanotom-s nano Computed Tomography (nanoCT) system (Phoenix x-ray, GE Measurement & Control; Wunstorf, Germany). The samples were scanned with 90 kV and 702 µA acquisition parameters. The software NRecon (Bruker) and Dataviewer (Bruker) were used for the image reconstruction. A circular area of 990 µm³ around the interface bone/implant was calculated based on the total volume of the analyzed area and CT-Analyzer (Bruker) and CT-Vol (Bruker) software were used for newly formed bone volume quantification.

2.7 | Flow cytometry

Flow cytometric analysis of implanted femur bone marrow cells was carried out at 1, 3, 5, and 7 days after the surgery (*n* = 5 animals). After euthanasia, the femurs with implants were dissected and the implants were removed by exposing proximal epiphysis to allow access to the implant. To flush the bone marrow cells, the femurs were placed in a 200 µl pipette tip with cut ends and placed in 1.5 ml microcentrifuge tubes. Femurs were centrifuged at 200 rpm for 5 min to collect the cells. The cells were then resuspended in 1 ml of MEM-alpha modified with Earle's Salts (MEM-α) (Gibco-Life, Grand Island, NY, United States) supplemented with 10% fetal bovine serum (Gibco) and antibiotic/antimycotic (penicillin/streptomycin/amphotericin B) (Sigma Chemical Co., St. Louis, MO, United States). Red blood cells were removed, and total cells were counted. One hundred thousand cells were centrifuged at 200 rpm for 3 min, and the cells were resuspended in 1 ml of PBS (10 ml of PBS, 100 mg BSA) in 5 ml round bottomed polystyrene tubes. The samples were immediately placed on ice and transported to the Biomedical Research Core Facilities at University of Michigan Medical School Office of Research and analyzed by MoFlo Astrios Cell Sorter (Life Science, Brea, CA, United States). For each time point, one positive animal which exhibited *Osterix* fluorescence and one negative animal were euthanized for controls.

2.8 | RNA isolation and analysis

Implant adherent cellular RNA was analyzed at 1, 3, 5, and 7 days after surgery (*n* = 5 animals). Implants were removed from the femurs and placed in 1 ml of TRIzol lysis reagent (Invitrogen, Carlsbad, CA, United States). We analyzed the cells adhering to the surface of the implants. The samples were kept frozen at –80°C for at least 24 h. Total RNA in the cell lysates was isolated according to the manufacturer's protocol and collected by ethanol precipitation. Total RNA was

quantified using a spectrophotometer (PowerWave HT—BioTek Instruments) and the Gen5™ program (BioTek Instruments). From each total RNA sample, cDNA was generated using SuperScript VILO cDNA Synthesis—Invitrogen) in a standard 20 μ l reaction using 100 ng of the total RNA. Subsequently, equal volumes of cDNA were used to program real-time PCR reactions specific for mRNAs encoding the early osteogenic markers: *Runx2*, *Osx*, *Satb2*, *Alp*, *Col1*, and *Prx1*; late osteogenic markers: *Dpm1*, *Bsp*, and *Ocn*; pro-inflammatory markers: *Tnf- α* and *Nos2* and anti-inflammatory marker *Il-10*. All primers were obtained from Qiagen (Qiagen, Germantown, MD, United States), and qPCR reactions were carried out

in an ABI 7900HT fast real-time (Applied Biosystems, Foster City, CA, United States). Relative mRNA abundance was determined by the $2^{-\Delta\Delta C_t}$ method and reported as fold induction. GAPDH abundance was used for normalization. Smooth samples at day 1 were used as the control group.

2.8.1 | Statistical analysis

Sample size was estimated in $n = 5$ based on a $p < .05$ and Power of 80%. Real time PCR results were shown as fold change by the $2^{-\Delta\Delta C_t}$

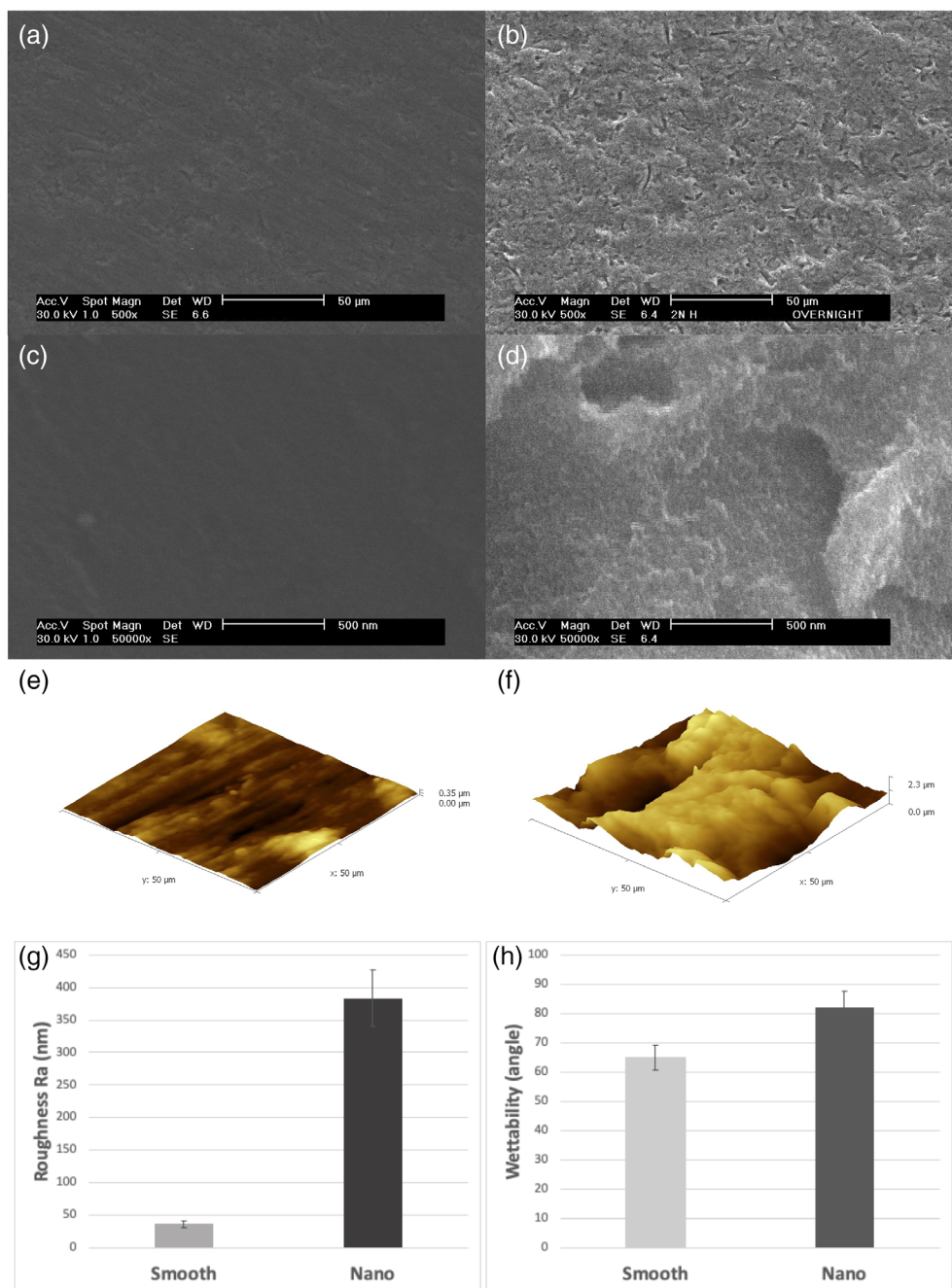


FIGURE 1 Surface characterization of prepared implants. Scanning electron microscopy (SEM) images of the evaluated surfaces: (A and C) Smooth, (B and D) nanoscale surface at different magnifications. 500 \times (A and B) and 50,000 \times (C and D) magnifications are shown. (E and F) Shows the 3D surface characterization from the atomic force microscopy (AFM). (G), roughness parameter (Ra) of each surface from the AFM is shown ($n = 3$). (H) Represents wettability for smooth and nano surfaces ($n = 3$)

method, in baseline 2, with smooth day 1 being used as the control. *t*-Test was used as a statistical test for comparison between the day 1 smooth control and the other groups.^{22,23} For the other tests, two-way analysis of variance (ANOVA) was used followed by the Tukey test when necessary. The software used for statistical analysis was Prism 6 (Graphpad Software Inc, La Jolla, CA, United States). For all statistical analyzes, the level of significance was set at $p < .05$.

3 | RESULTS

3.1 | Surface analysis—Scanning electron microscopy

Evaluation of prepared implants demonstrated the topographies unique to both the smooth ($R_a = 36 \pm 5.7$ nm) and the nanoscale ($R_a = 384 \pm 43.1$ nm) implants (Figure 1). Wettability measures of Ti

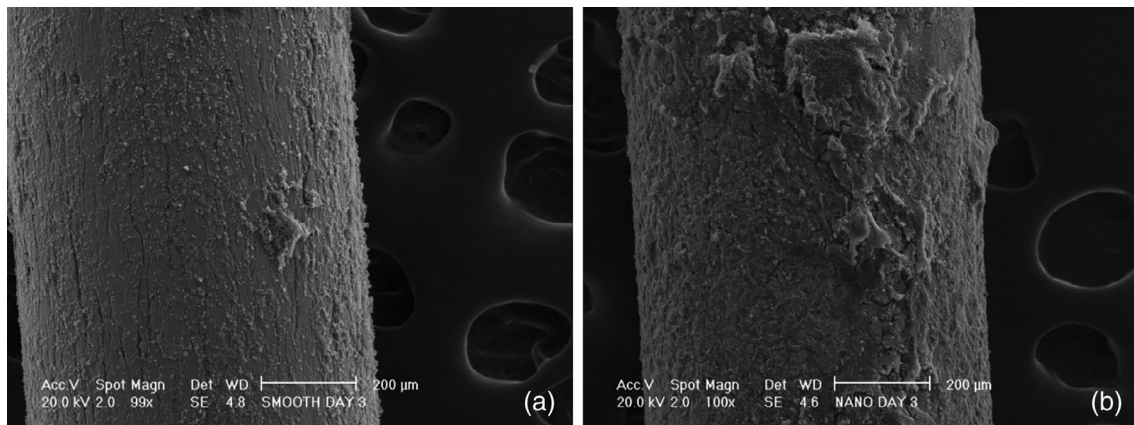


FIGURE 2 Low resolution images of titanium implants after removal from bone at 7 days. (A) Smooth surface implant with minimal residual tissue attached. (B) Nanoscale surfaces with abundant residual tissue attached

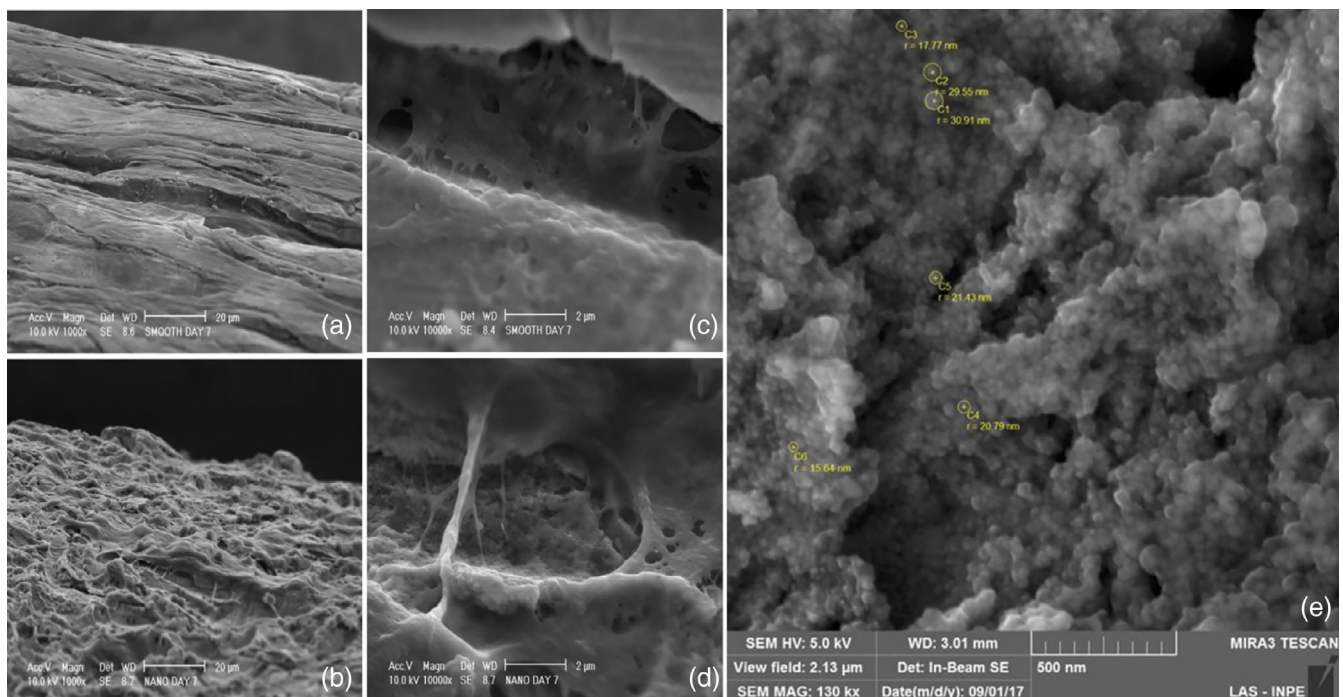


FIGURE 3 High resolution images of titanium implants after removal from bone at 7 days. Scanning electron micrographs of the smooth (A and C) and nano (B and D) surfaces. At 1,000 \times magnification (A and B) it was possible to see the differences between surfaces. At magnification 10,000 \times (C and D) it was possible to observe cell/surface interactions. An increased number of lamellipodia and filopodia were observed on the nano surface. (E) At 13,000 \times it was possible to see rounded nanostructures with an average equivalent diameter of approximately 20 nm. Scale bar (A) and (B) = 20 μm, Scale bar (C) and (D) = 2 μm, Scale bar (E) = 500 nm

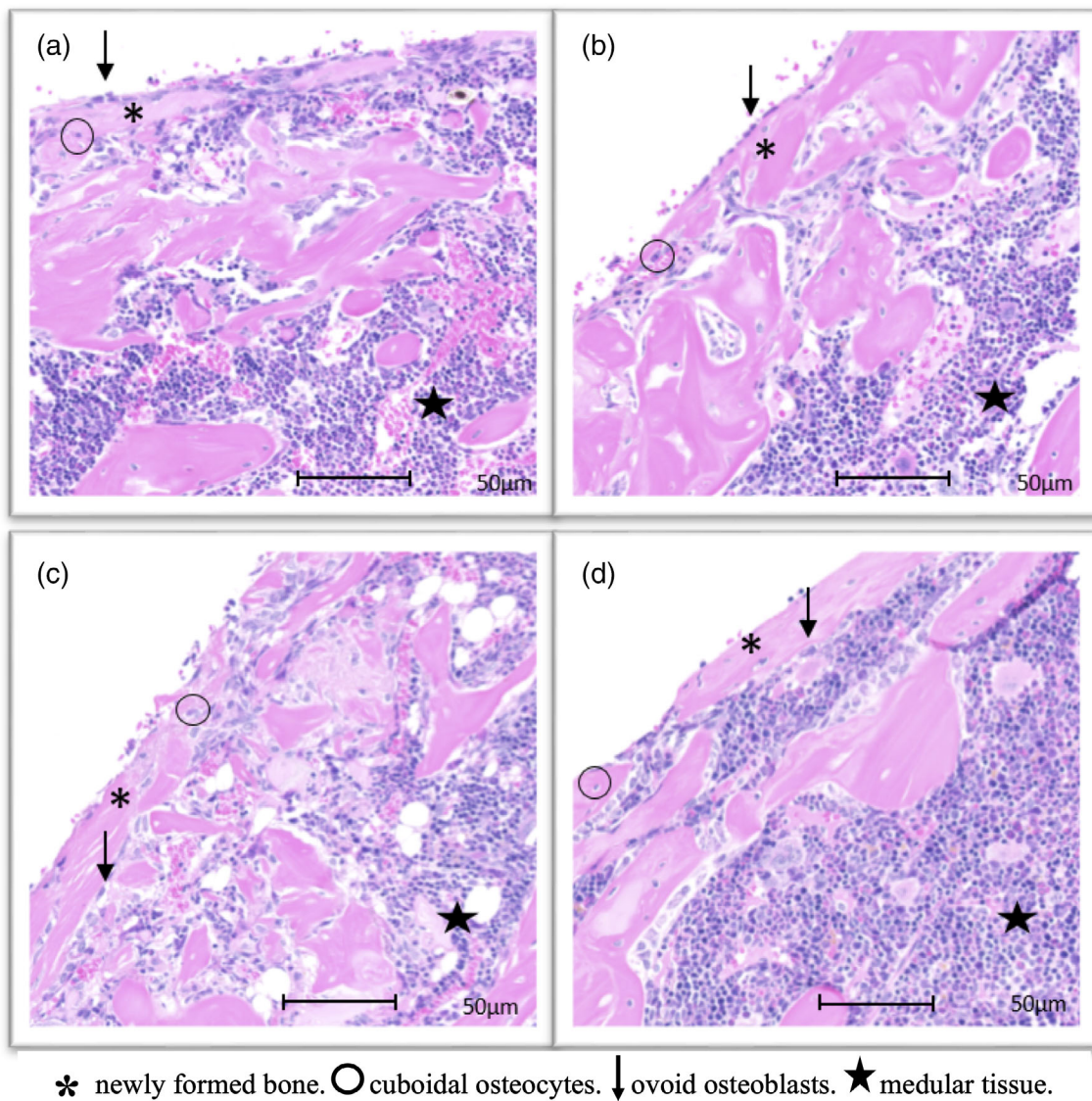


FIGURE 4 Histological evaluation of newly formed bone-to-implant interfaces. Early osseointegration at 7 days at smooth surface (A) and nano surface (B). Note the formation of immature and non-lamellar bone at the two surfaces with the presence of cuboidal osteoblasts in a single row bordering the trabeculae of new bone, and osteocytes trapped in the osteoid matrix. Extended interfacial bone formation is observed at 14 days at smooth surface (C) and nano surface (D) implant interfaces. More extensive, non-lamellar bone formation is observed across these surfaces ($n = 5$)

disks prepared in parallel indicated greater hydrophobicity of the nanoscale versus the smooth surface disks (82° vs. 65° ; Figure 1H). SEM was also used to illustrate the residual tissues attached to both implant surfaces following removal at 7 days (Figure 1A,B). Low magnification SEM images revealed less adherent tissue on smooth versus nano surfaces (Figure 2A,B). At high magnification (Figure 3), fewer lamellipodia and filopodia attachments were observed at the smooth (Figure 3C) than at the nanoscale surface (Figure 3D). This indicates differential attachment and spreading at the two different surfaces. Nano surface revealed the conservation of nano-scale features and at higher resolution, the presence of discrete 20–30 nm nanofeatures were observed (Figure 1B,D,E).

3.2 | Histological assessment of interfacial bone formation

Titanium implant placement in the femur elicits a bone forming response. At 7 days the histologic evaluation demonstrated bone adjacent to the implant was immature and non-lamellar for the two surfaces studied (Figure 4A,B). Active bone formation was evidenced by the presence of cuboidal osteoblasts in a single row bordering the trabeculae of new bone, with basophilic cytoplasm indicating cells active in the process of bone formation. Cuboidal osteocytes were observed randomly trapped in the osteoid matrix. At 14 days (Figure 4C,D), continued development of the bone-to-implant surface

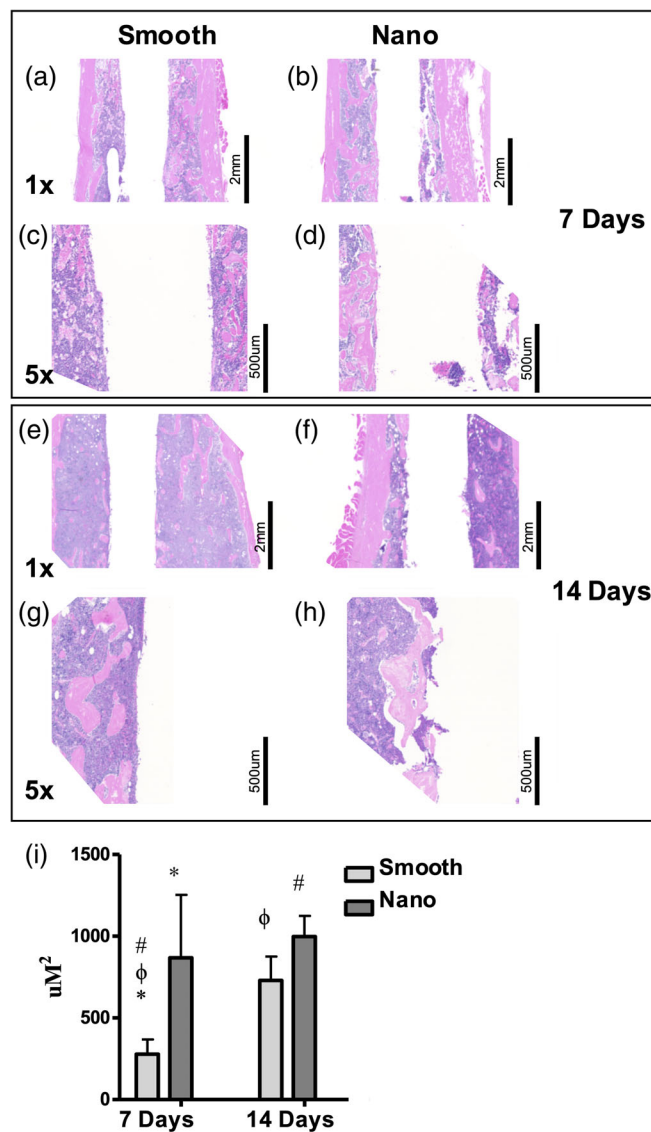


FIGURE 5 Decalcified histology sections (H&E staining) at Implants. (A–H) Assessment of bone-to-implant contact after 7 days (A–D) and 14 days (E–H) at smooth (A, C, E, and G) and nano (B, D, F, and H) surface implants. (I) Quantification of bone-implant contact at smooth versus nano surface implants. The bone contact in μm^2 on smooth and nano Ti implant surface at days 7 and 14. Statistical differences were observed between surfaces (day 7) and periods studied ($p < .05$) ($n = 5$)

was revealed. At 21 days, the removal of the implant disrupted the interface that prevented interfacial analysis and suggested by 21 days the development of an osseointegrated interface (not shown) at both implant surfaces. Quantification at the cross-section area after removal of the implant allowed to observe differences in BIC at 7 and 14 days. Figure 5 represents BIC. Statistically significant differences in BIC were observed by two-way ANOVA between the two surfaces and time points followed by Tukey test ($p < .05$) (Figure 5I). Nano surface showed higher BIC values than smooth surface at 7 days for both timepoints (nano 7 days and nano 14 days). Smooth surface at 14 days also showed Ti improved BIC compared to smooth 7 days.

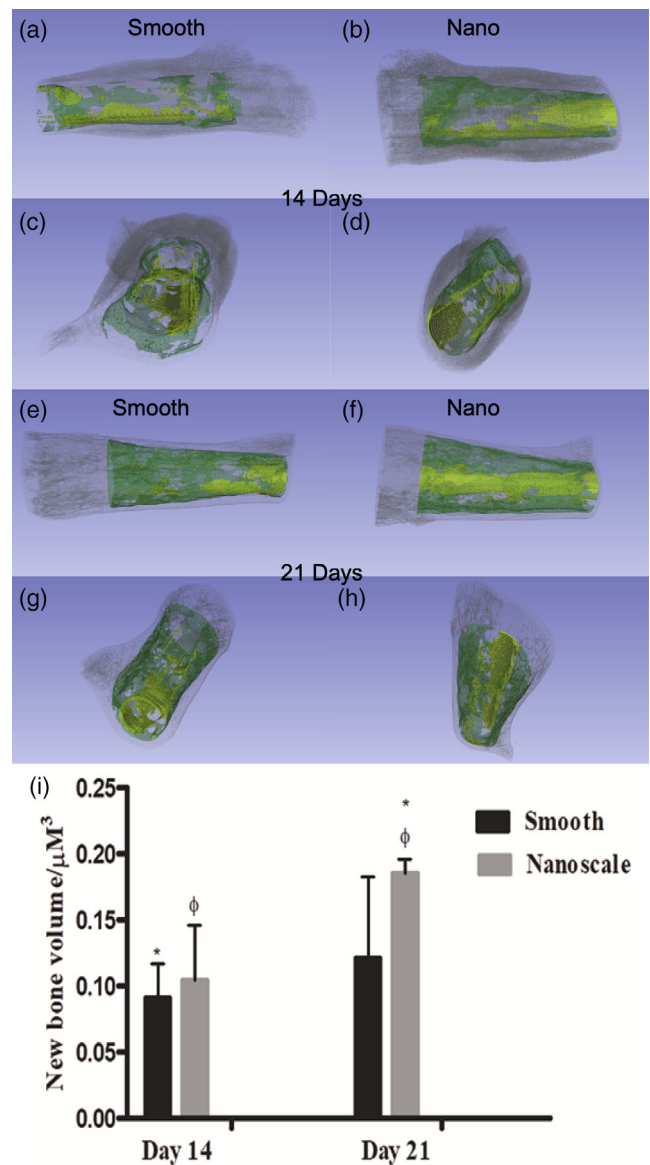


FIGURE 6 NanoCT imaging of bone formation at implants. (A–H) Qualitative assessment by nanoCT reconstruction of osseointegration after 14 days (A–D) and 21 days (E–H) at smooth (A, C, E, and G) and nano (B, D, F, and H) surface implants. Yellow represents new bone in contact with the implant. Green represents the remaining bone marrow trabecular bone. Gray shows the cortical bone. (I) Quantification of bone formation at smooth versus nano surface implants (yellow areas on images above). The bone volume formed in μm^3 on smooth and nano Ti implant surface at days 14 and 21. Statistical differences were observed between surfaces (day 14) and periods studied ($p < .05$) ($n = 5$)

3.3 | NanoCT

NanoCT was used to quantify the bone-to-implant contact and bone volume formed at 14 and 21 days following placement in the femurs. Figure 6A,C represent the image reconstructions for the day 14 smooth implants and Figure 6B,D represent the reconstructions for the day 14 nanosurface implants. Figure 6E,G shows reconstitution on day

21 of the smooth implants, while Figure 6F,H represent 21-day nanosurface implant image reconstructions. New bone (visualized here in yellow) was observed at all implants. The bone marrow stroma is colored green, while the color gray shows the compact bone. The measure

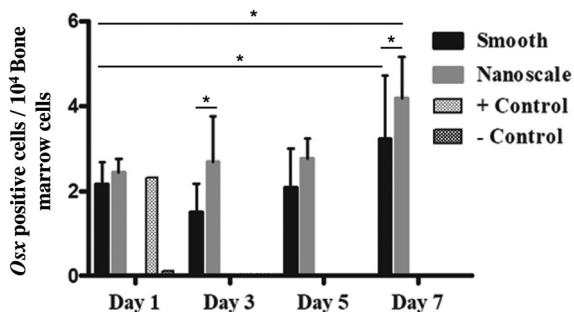


FIGURE 7 Flow cytometric analysis of *Osterix* expressing cells in implanted bones. Flow cytometry graph showing the quantification of cells expressing the *Osterix* gene after 1, 3, 5, and 7 days of implantation. Positive and negative mice were used as control. There is a trend indicating that more *Osterix* positive cells (per 10⁴ bone marrow cells) are present on nanoscale surface implants than smooth surface implants after days 3–7 ($N = 5$). No statistical differences were found between the groups and periods analyzed ($n = 5$)

of newly formed bone was calculated and plotted for both time point and surfaces. At day 14, the quantification of the newly formed (yellow) showed a modest increase in bone volume at the nano implant interface compared to the smooth implant interface. At day 21, greater new bone was observed at the nano versus smooth implant. Statistically significant differences were observed by two-way ANOVA followed by Tukey test ($p < .05$) between the two time points for new bone volume. Statistically significant differences were observed between nano day 21 with nano day 14 ($p < .05$) and smooth day 14 ($p < .05$) (control group) (Figure 6I). No statistically significant difference was found between smooth day 14 and smooth day 21. Suggested is the acceleration of bone accrual at the nano surface implants.

3.4 | Flow cytometry

OSX-Cherry transgenic mice used in this study permitted direct assessment of *Osterix* gene expression with respect to implant surface topography. The low number of isolated cells adherent to the retrieved implants precluded quantitative analysis of the adherent cells by flow cytometry. Analysis of *Osterix* expression in residual peripheral bone was performed. Figure 6 shows number of *Osx* positive cells/10⁴ bone marrow cells. The number of *Osterix* expression

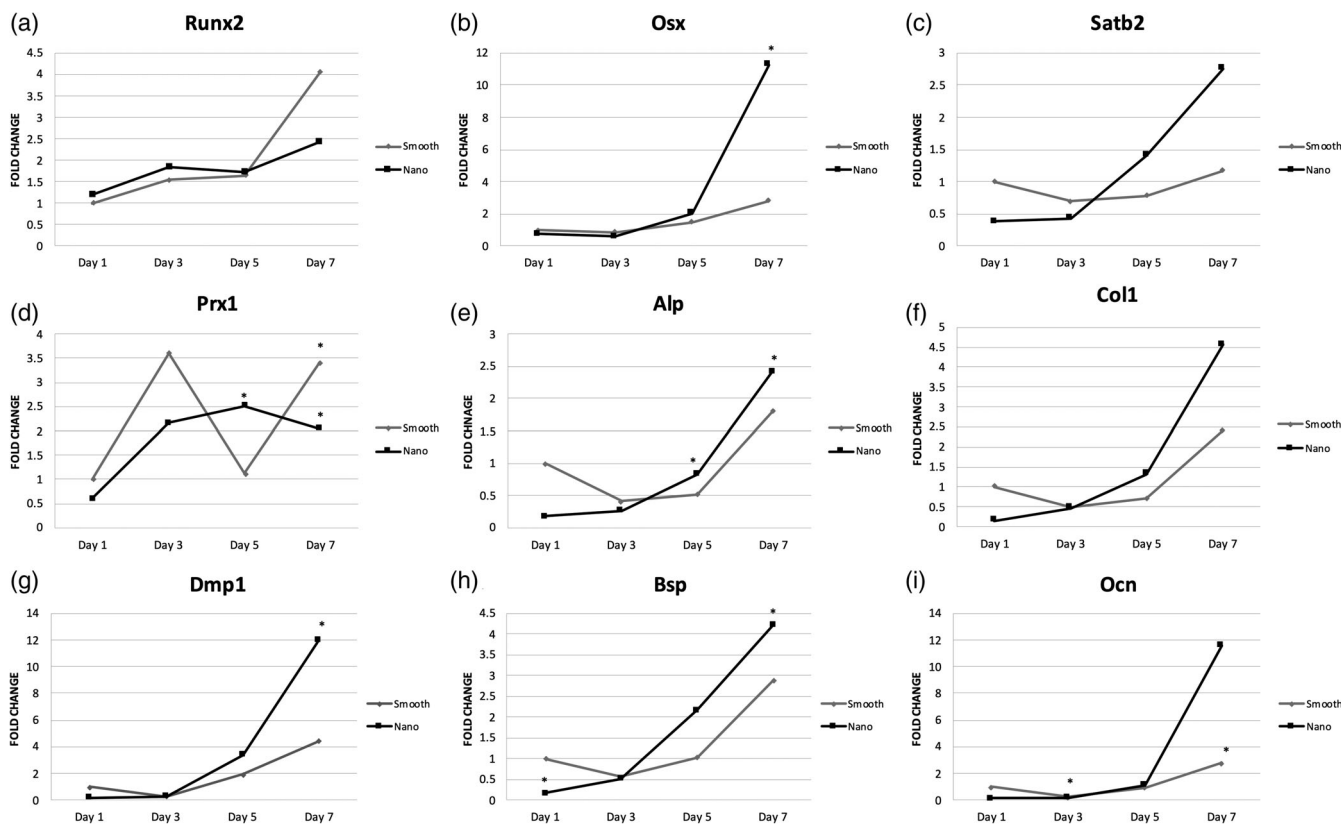


FIGURE 8 Osteoinductive and osteogenic gene expression in implant adherent cells. Expression levels (fold change) of osteoinductive and osteogenic genes were compared between cells adherent to smooth and nano surfaces. (A) *Runx2*; (B) *Osx*; (C) *Satb2*; (D) *Prx1*; (E) *Alp*; (F) *Col1*; (G) *Dmp1*; (H) *Bsp*; and (I) *Ocn*. Total RNA was isolated from the cells at 1, 3, 5, and 7 days of the mice femurs. The results are shown as fold change ($2^{-\Delta\Delta C_t}$ method, baseline = smooth Day 1, $n = 5$). *Statistically significant difference when compared with the baseline ($p < .05$) ($n = 5$)

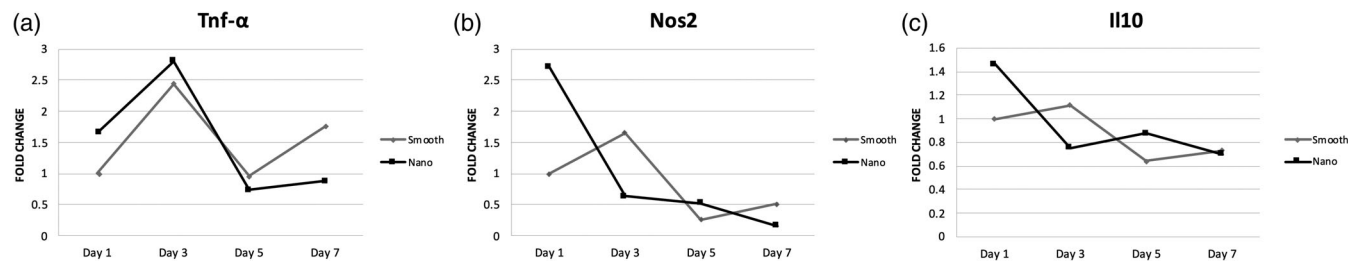


FIGURE 9 Immunomodulatory gene expression in smooth and nanoscale implant adherent cells. Total RNA was isolated from cells at 1, 3, 5, and 7 days of the mice femurs and RT-PCR was performed for (A) *Tnfα*, (B) *Nos2*, and (C) *IL-10* mRNA expression. Expression levels (fold change) compared between smooth and nano surfaces for inflammatory genes demonstrate downregulation of inflammation-associated gene expression at both surfaces. The results are shown as fold change ($2^{-\Delta\Delta Ct}$ method, baseline = smooth Day 1, $n = 5$, *Statistically significant difference when compared with baseline ($p < .05$) ($n = 5$))

positive cells was greater in forming bone/bone marrow associated with the nano surface implants, when compared to smooth surface implants, and the positive control group at all-time points. The smooth group presented higher numbers of *Osterix* expressing cells compared to the positive control on day 7. Statistically significant differences for *Osx* positive cells were found between smooth and nano surfaces at day 3 and day 7 ($p < .05$). At day 7 the number of *Osx* positive cells on the smooth and nano surfaces were also statistically different from smooth at day 1 (control group) ($p < .05$) (Figure 7).

3.5 | Gene expression analysis (qPCR)

The tissues remaining on the implant surface after removal were analyzed by qPCR. The results are presented as relative levels of expression in relation to the smooth day 1 as control group (Method $2^{-\Delta\Delta Ct}$, $n = 5$ for each time point). Expression of the osteoinductive transcription factor *Runx2* mRNA (Figure 8A) was enhanced by day 7 within tissue adherent to both implant surfaces; *Runx2* expression in smooth surface implant adherent cells was greater than for nano surface implant adherent cells (4-fold vs. 2.5-fold). Notably, cells in forming tissues adherent to the nano surface implant demonstrated elevated and accelerated expression of *Osterix* when compared to smooth surface implants at all-time points (Figure 7B) and was nearly 6-fold higher by day 7. On the smooth surface, *Osterix* expression was not significantly elevated at day 7, with values close to the baseline. The surface-specific expression of *Runx2* (greater on smooth surfaces at day 7) and *Osterix* (greater on nanosurfaces at day 7) illustrate the possibility that these surfaces influence different osteoinductive pathways that both lead to bone formation. The high level of *Osterix* expression is associated with greater bone formation and is underscored by *Cherry* expression in this transgenic mouse model.

Other bone-specific protein encoding mRNA levels were also upregulated in tissues adherent to the nano surface implants. *Alp* (Figure 8E), a marker that indicates osteoblast differentiation in early-stage osteogenesis, showed as 2.5-fold upregulated on the nanoscale at days 5 and 7. The smooth surface showed low *Alp* expression in time points. *Col1* expression (Figure 8F) at day 7 was higher on the

nanoscale surface (4.5-fold) compared to the smooth surface (2.5-fold). *Satb2* (Figure 8C) was expressed at increased levels (2.5-fold) only on the nanoscale surface at day 7. *Prx1* (Figure 8D) showed increased expression on the smooth surface at 3 and 7 days. On the nanoscale surface, this gene showed a more constant expression pattern with values above the baseline from day 3 (2.5-fold upregulated at day 5). The osteogenic protein mRNAs *Dmp1* (Figure 8G) and *Bsp* (Figure 8H) showed elevated steadystate levels on the nanoscale surfaces after 5 days in vivo. By day 7, *Dmp1*, *Bsp*, and *Ocn* demonstrated elevated expression on both surfaces (Figure 8G–I). The shift of the *Dmp1* and *Bsp* expression curves to the left indicate an acceleration of osteogenesis mediated by cells adherent to the nanoscale surfaces in vivo.

Immunomodulation is known to occur at implant surfaces.²⁴ To additionally examine the role of implant topography on this process, we measured expression of inflammation-associated protein encoding mRNAs *Tnfα*, *Nos2*, and *Il10* in tissues adherent to these retrieved implant surfaces. *Tnf-α* (Figure 9A) showed low levels of gene expression at both surfaces. At day 3, there was an increase in gene expression for *Tnf-α* for both surfaces, with the nano surface showing 3-fold change, and the smooth surface showing as 2.5-fold increase. At days 5 and 7 the levels of *Tnf-α* for the two surfaces were below baseline, illustrating the immunomodulation that occurs with implant-adherent inflammatory cells. *Nos2* (Figure 9B) showed elevated for the nanoscale surface (3-fold) while smooth surface showed low gene expression. The anti-inflammatory gene, *Il-10* (Figure 9C) showed low expression for all time points on both surfaces.

4 | DISCUSSION

Surface topographic promotion of osseointegration is dependent on the ability to induce differentiation of pluripotent mesenchymal stem cells to the osteoblast lineage and to stimulate matrix secretion by osteoblasts.^{1,25,26} This study demonstrates that surface topography differentially influenced osseointegration, in part by enhancing new bone formation. Presenting osteoinductive characteristics providing a biological stimulus for recruitment of mesenchymal stem cells and its

differentiation into osteoblasts. *Osterix* gene expression and known downstream target gene expression. This affirms that nanoscale topographic features alter adherent cell function including the promotion of differentiation of mesenchymal stem cells into osteoblasts.^{21,27,28} Here, we evaluated the on impact on the osseointegration process of a hybrid topographic surface created by superimposition of nanoscale topography onto micron rough cp titanium implant surfaces using a validated laboratory process.²⁹ In this study our control surface was the smooth topography as our previous in vitro study demonstrated similar results to a micron-rough surface.⁸ SEM and AFM measurements demonstrated the current implant nanoscale features conform to a range of nanotopographies known to positively influence osseointegration.^{1,6} The present in vivo study affirms the distinct impact of nanoscale topography on cell adhesion, osteoinduction, osteogenesis, and bone-to-implant interface formation.

Implant adherent cells are informed by topography. While this is visualized by changes in cell shape, numerous reports demonstrate that topography is an important environmental cue that informs cell function. Here, cell adhesion and spreading was illustrated by post-retrieval SEM analyses (Figure 2) and validated the different morphology of cells adherent to smooth versus nanoscale hybrid surfaces.

Mesenchymal stem cell/osteoprogenitor cell osteoinduction is a well-defined process involving the master regulatory transcription factors, *Runx2*, and *Osterix* (*Sp7*). The main gene indicated as essential for mesenchymal stem cells in osteoprogenitor lineage is *Runx2*, whose presence excludes the possibility of these cells becoming adipocytes or chondrocytes.³⁰ *Osterix* is necessary in the process of osteoinduction and its overexpression eliminates the possibility of pre-osteoblasts being differentiated into chondrocytes.³¹ Together, *Runx2*, and *Osterix* instruct the differentiation of pre-osteoblasts into osteoblasts in the process of bone formation. We and others have observed distinct effects of surface topography effects on implant adherent cell *Runx2* and *Osterix* expression that suggests that topography may differentially influence the *Runx2* and *Osterix* signaling pathways.^{12,29,32}

Osterix expression differs at smooth and nanoscale endosseous implants in the *Osterix-Cherry* mouse model and this was observed at multiple levels, including flow cytometric analysis of surrounding bone cell phenotype and RT-PCR quantification of *Osterix* gene expression in implant adherent cells. By use of this transgenic reporter mouse model, the direct observation of *Osterix* expressing osteoprogenitors was confirmed further affirmed that *Osterix* expression is higher in tissues adherent to and adjacent to the nano surface implant when compared to the smooth surface implant. There is consensus observations that implant topography at the micro/nano levels positively influence *Osx* gene expression,^{12,29} The earlier and more profound induction of *Osx* gene expression versus *Runx2* expression observed in this study (upregulation of *Osx* at day 5 versus *Runx2* at day 7; *Osx* expression almost 5 times greater than *Runx2*) again implies that *Osx* is differentially and positively regulated by nanoscale topographic features on implants. These results are consistent with previous studies that evaluate the effect of nanostructures on hMSC (human mesenchymal stem cells) differentiation where increased *Runx2* expression was

delayed with respect to *Osx* expression.^{29,32-34} Both of these genes drive early mesenchymal stem cell osteoblastic differentiation and may serve to accelerate the osseointegration process in surface topography-dependent ways.³⁵

Satb2 encodes another transcription factor that is involved in the early process of osteogenesis. *Satb2* can synergize, amplify, and thus, exponentially increase the activity of multiple osteogenic factors *Runx2* and *Osx* to positively influence the expression of bone marker genes, such *Bsp* and *Ocn*.³⁶ On the tested implant surfaces, *Satb2* mRNA expression increased in accordance with increased *Osx* expression observed for cells adherent to nanoscale implant surfaces but not smooth surfaces. This is consistent with *Satb2* functioning downstream of *Osx* expression.³⁰ This observation of high expression of *Osx* and *Satb2* on nanoscale implant surfaces may underscore other measured changes in osteogenic gene expression. In studies of *Satb2* function, *Satb2* knockdown by siRNA inhibited *Osx*-induced gene expression including *Alp*, *Ocn*, and *Bsp*. Here, we observe parallel impact of surface topography on adherent cell *Osx* and *Satb2* expression as well as known downstream targets such as *Alp*, *Ocn*, and *Bsp* expression. Importantly, the present correlative study using *Osterix-Cherry* expression further implicates *Osx* as a central mediator of bone formation that is influenced by nanoscale surface topography.

In the early events of bone/wound healing after implant placement, the recruitment of the inflammatory cells and mesenchymal stem cells are part of the cellular wound healing response.³⁷ The rapid physiological resolution of inflammation is necessary for bone healing, thus an increase of the pro-inflammatory as well as anti-inflammatory genes is necessary in the early and late stages of implantation respectively, since the presence of pro- and anti-inflammatory cytokines expressed at the same time contribute to a poorly balanced environment for proper wound healing to occur.³⁸ In our study, we observed early reduction in expression of pro-inflammatory genes *Tnf- α* and *Nos2* only on the nanoscale surface. This implies that nano surface implants may benefit from earlier or more profound immunomodulation that advances osteogenesis and wound healing. These findings are consistent with other reports concerning nanotopography and osseointegration/bone formation.²⁶

Immature osteoblasts express *Alp* and *Col*, and in this study, earlier and greater mRNA expression of these genes were observed in cells adherent to nanosurfaces. Following the continued osteogenesis process, we observed expression of both *Col* and *Bsp*, followed by a later expression of *Ocn*. This sequence is consistent with phases of bone-specific gene expression during osteogenesis.^{32,39} *Dmp1* is expressed by osteocytes and influences mineralization.^{27,40} Expression of *Dmp1* at these implants was interestingly observed relatively early (at day 5) and is consistent with previous studies of hybrid topography.⁴¹ Other genes of interested included *Prx1*. The understanding of the role of *Prx1* in osseointegration is still limited.²⁰ *Prx1* expressed in periosteal cells differentiated into osteoblasts, which are present in the fracture callus.⁴² *Prx1* expression may represent additional evidence of the active osteoinduction on implant adherent cells. Suggested is an acceleration of the later, committed phases of osteogenesis and initial mineralization at nanoscale surfaces. In aggregate,

the mRNA expression patterns indicate a dynamic process that is influenced by topography at multiple stages including immunomodulation, MSC recruitment and differentiation into osteoblasts. Followed by bone matrix production and mineralization.

We directly measured *Osterix* gene expression by flow cytometric analysis of the Cherry expression in bone cells surrounding the implants.³⁶ The quantitative analysis by flow cytometry of the cells extracted from the bones of implanted femurs enabled the direct evaluation of *Osterix* gene regulation. In this analysis, greater numbers of Cherry-positive cells were observed in the femurs implanted with nanoscale implants. Implant adherent cells were not included in flow cytometric analysis due to the low number of adherent cells isolated following implant removal. The modest elevation in Cherry-positive cells isolated from femurs implanted with nanoscale implants indicates that both adherent cells and local cells are influenced by surface topography. This further implicates the paracrine function of adherent cells in control of bone physiology following implantation.

NanoCT quantification of the bone to implant contact formed demonstrated that greater osseointegration occurred at the nanoscale implant surface. The earlier and greater accrual of bone at the nanosurface implants affirms previous studies involving various nanoscale surfaces prepared by HF treatment, Alumina treatment, or nanotube development.^{12,43,44} Conventional quantification using ground sections was not performed in order to permit histological determination of *Osterix*-Cherry expression.

Histological analysis of femurs following implant removal allowed us for analysis of bone to implant contact based on the cross-sectioned implant interface. It also allowed the visualization of newly formed bone and indicated that healthy bone and bone marrow was present surrounding both implant surfaces (Figures 4 and 5). For quantitative analysis of bone formation at the implant interface, NanoCT revealed greater bone-to implant contact at nano surface implants with statistical differences for the nano surface at 21 days compared to the smooth and nano surfaces at 14 days (Figure 6). This demonstrates a progressive increase of new bone formation on this surface.

There are several potential limitations of this study. Ground sections were not used to affirm the microCT quantification of bone to implant contact. While increasing bone to implant contact has been associated with increased mechanical interaction of endosseous implants with bone, mechanical testing of the present implants was not performed. In this article the authors did not further evaluate how different surface topographies affect protein adsorption and conformation in relation to changes in wettability.

5 | CONCLUSION

This in vivo study demonstrates that *Osterix* gene expression is a component of the osteoinductive process at dental implants and is preferentially influenced by nanoscale topography of the endosseous implant. The affirmed role of *Osx* gene regulation and its downstream targets in accelerating and increasing the formation of bone at

endosseous implant surfaces indicates that it is a molecular target for further enhancement of implant surface topography.

ACKNOWLEDGMENTS

This work was supported by an Implant Innovation Award from the Osseointegration Foundation and International Association for Dental Research (IADR). Research reported in this publication was supported by the National Institute of Arthritis and Musculoskeletal and Skin Diseases of the National Institutes of Health under Award Number P30 AR069620. The content is solely the responsibility of the authors and does not necessarily represent the official views of the National Institutes of Health.

DATA AVAILABILITY STATEMENT

Data available in the article

ORCID

Lais Morandini Rodrigues  <https://orcid.org/0000-0003-2472-2246>

Elis A. Lima Zutin  <https://orcid.org/0000-0002-7585-1868>

Elisa M. Sartori  <https://orcid.org/0000-0002-3423-3617>

Fabio A. P. Rizzante  <https://orcid.org/0000-0002-4123-5637>

Daniela B. S. Mendonça  <https://orcid.org/0000-0003-0658-1558>

Paul H. Krebsbach  <https://orcid.org/0000-0001-9062-4981>

Karl J. Jepsen  <https://orcid.org/0000-0002-2903-9940>

Lyndon F. Cooper  <https://orcid.org/0000-0002-6577-781X>

Luana M. R. Vasconcelos  <https://orcid.org/0000-0003-4344-0578>

Gustavo Mendonça  <https://orcid.org/0000-0003-2290-4046>

REFERENCES

- Mendonça G, Mendonça DBS, Aragão FJL, Cooper LF. Advancing dental implant surface technology - From micron- to nanotopography. *Biomaterials*. 2008;29(8):3822-3835. <https://doi.org/10.1016/j.biomaterials.2008.05.012>
- Chakravorty N, Ivanovski S, Prasadam I, Crawford R, Oloyede A, Xiao Y. The microRNA expression signature on modified titanium implant surfaces influences genetic mechanisms leading to osteogenic differentiation. *Acta Biomater*. 2012;8(9):3516-3523.
- Cooper LF. Biologic determinants of bone formation for osseointegration: clues for future clinical improvements. *J Prosthet Dent*. 1998;80(4):439-449.
- Meirelles L, Arvidsson A, Andersson M, Kjellin P, Albrektsson T, Wennerberg A. Nano hydroxyapatite structures influence early bone formation. *J Biomed Mater Res A*. 2008;87(2):299-307.
- Gittens RA, Scheideler L, Rupp F, et al. A review on the wettability of dental implant surfaces II: biological and clinical aspects. *Acta Biomater*. 2014;10(7):2907-2918.
- Liu Y, Luo D, Wang T. Hierarchical structures of bone and bioinspired bone tissue engineering. *Small*. 2016;12(34):4611-4632.
- Gittens RA, Olivares-Navarrete R, Cheng A, et al. The roles of titanium surface micro/nanotopography and wettability on the differential response of human osteoblast lineage cells. *Acta Biomater*. 2013;9(4):6268-6277.
- Mendonça G, Mendonça DB, Aragão FJ, Cooper LF. The combination of micron and nanotopography by H(2)SO(4)/H(2)O(2) treatment and its effects on osteoblast-specific gene expression of hMSCs. *J Biomed Mater Res A*. 2010;94(1):169-179.
- Kubo K, Tsukimura N, Iwasa F, et al. Cellular behavior on TiO2 nanonodular structures in a micro-to-nanoscale hierarchy model. *Biomaterials*. 2009;30(29):5319-5329.

10. Mendes VC, Moineddin R, Davies JE. The effect of discrete calcium phosphate nanocrystals on bone-bonding to titanium surfaces. *Biomaterials*. 2007;28(32):4748-4755.
11. Karazisis D, Petronis S, Agheli H, et al. The influence of controlled surface nanotopography on the early biological events of osseointegration. *Acta Biomater*. 2017;53:559-571.
12. Guo J, Padilla RJ, Ambrose W, de Kok IJ, Cooper LF. The effect of hydrofluoric acid treatment of TiO₂ grit blasted titanium implants on adherent osteoblast gene expression in vitro and in vivo. *Biomaterials*. 2007;28(36):5418-5425.
13. Webster TJ, Ergun C, Doremus RH, Siegel RW, Bizios R. Enhanced functions of osteoblasts on nanophase ceramics. *Biomaterials*. 2000; 21(17):1803-1810.
14. Kulkarni M, Mazare A, Gongadze E, et al. Titanium nanostructures for biomedical applications. *Nanotechnology*. 2015;26(6):062002.
15. Yin C, Zhang Y, Cai Q, et al. Effects of the micro-nano surface topography of titanium alloy on the biological responses of osteoblast. *J Biomed Mater Res A*. 2017;105(3):757-769.
16. Huang Q, Elkhoory TA, Liu X, et al. Effects of hierarchical micro/nanotopographies on the morphology, proliferation and differentiation of osteoblast-like cells. *Colloids Surf B Biointerfaces*. 2016;145:37-45.
17. Gulati K, Prideaux M, Kogawa M, et al. Anodized 3D-printed titanium implants with dual micro- and nano-scale topography promote interaction with human osteoblasts and osteocyte-like cells. *J Tissue Eng Regen Med*. 2017;11(12):3313-3325.
18. Marcatti Amarú Maximiano W, Marino Mazucato V, Tambasco de Oliveira P, Célia Jamur M, Oliver C. Nanotextured titanium surfaces stimulate spreading, migration, and growth of rat mast cells. *J Biomed Mater Res A*. 2017;105(8):2150-2161.
19. de Oliveira PT, Nanci A. Nanotexturing of titanium-based surfaces upregulates expression of bone sialoprotein and osteopontin by cultured osteogenic cells. *Biomaterials*. 2004;25(3):403-413.
20. Thalji G, Gretzer C, Cooper LF. Comparative molecular assessment of early osseointegration in implant-adherent cells. *Bone*. 2013;52(1): 444-453.
21. Bryington M, Mendonça G, Nares S, Cooper LF. Osteoblastic and cytokine gene expression of implant-adherent cells in humans. *Clin Oral Implants Res*. 2014;25(1):52-58.
22. Yuan JS, Reed A, Chen F, Stewart CN Jr. Statistical analysis of real-time PCR data. *BMC Bioinformatics*. 2006;7:85.
23. Wescott DC, Pinkerton MN, Gaffey BJ, Beggs KT, Milne TJ, Meikle MC. Osteogenic gene expression by human periodontal ligament cells under cyclic tension. *J Dent Res*. 2007;86(12):1212-1216.
24. Wang J, Meng F, Song W, et al. Nanostructured titanium regulates osseointegration via influencing macrophage polarization in the osteogenic environment. *Int J Nanomedicine*. 2018;13:4029-4043.
25. Boyan BD, Cheng A, Olivares-Navarrete R, Schwartz Z. Implant surface design regulates mesenchymal stem cell differentiation and maturation. *Adv Dent Res*. 2016;28(1):10-17.
26. Bressan E, Sbricoli L, Guazzo R, et al. Nanostructured surfaces of dental implants. *Int J Mol Sci*. 2013;14(1):1918-1931.
27. Harris SE, Gluhak-Heinrich J, Harris MA, et al. DMP1 and MEPE expression are elevated in osteocytes after mechanical loading in vivo: theoretical role in controlling mineral quality in the perilacunar matrix. *J Musculoskelet Neuronal Interact*. 2007;7(4):313-315.
28. Lu X, Beck GR Jr, Gilbert LC, et al. Identification of the homeobox protein Prx1 (Mhox, Prrx-1) as a regulator of osterix expression and mediator of tumor necrosis factor alpha action in osteoblast differentiation. *J Bone Miner Res*. 2011;26(1):209-219.
29. Mendonça G, Mendonça DBS, Aragão FJL, Cooper LF. The combination of micron and nanotopography by H₂SO₄/H₂O₂ treatment and its effects on osteoblast-specific gene expression of hMSCs. *J Biomed Mater Res A*. 2010;94A(1):169-179.
30. Tang W, Li Y, Osimiri L, Zhang C. Osteoblast-specific transcription factor Osterix (Osx) is an upstream regulator of Satb2 during bone formation. *J Biol Chem*. 2011;286(38):32995-33002.
31. Nakashima K, Zhou X, Kunkel G, et al. The novel zinc finger-containing transcription factor osterix is required for osteoblast differentiation and bone formation. *Cell*. 2002;108(1):17-29.
32. Stein GS, Lian JB, Stein JL, van Wijnen AJ, Montecino M. Transcriptional control of osteoblast growth and differentiation. *Physiol Rev*. 1996;76(2):593-629.
33. Sartori EM, Magro-Filho O, Mendonça D, Li X, Fu J, Mendonça G. Modulation of micro RNA expression and osteoblast differentiation by Nanotopography. *Int J Oral Maxillofac Implants*. 2018;33(2):269-280.
34. Aubin JE. Bone stem cells. *J Cell Biochem*. 1998;72(Suppl. 30-31):73-82.
35. Isa ZM, Schneider GB, Zaharias R, Seabold D, Stanford CM. Effects of fluoride-modified titanium surfaces on osteoblast proliferation and gene expression. *Int J Oral Maxillofac Implants*. 2006;21(2):203-211.
36. Telford WG, Hawley T, Subach F, Verkhusha V, Hawley RG. Flow cytometry of fluorescent proteins. *Methods*. 2012;57(3):318-330.
37. Berglundh T, Abrahamsson I, Lang NP, Lindhe J. De novo alveolar bone formation adjacent to endosseous implants. *Clin Oral Implants Res*. 2003;14(3):251-262.
38. Eming SA, Martin P, Tomic-Canic M. Wound repair and regeneration: mechanisms, signaling, and translation. *Sci Transl Med*. 2014;6(265):265sr6.
39. Aubin JE. Osteoprogenitor cell frequency in rat bone marrow stromal populations: role for heterotypic cell-cell interactions in osteoblast differentiation. *J Cell Biochem*. 1999;72(3):396-410.
40. Bhatia A, Albazzaz M, Espinoza Orías AA, et al. Overexpression of DMP1 accelerates mineralization and alters cortical bone biomechanical properties in vivo. *J Mech Behav Biomed Mater*. 2012;5(1):1-8.
41. Thalji GN, Nares S, Cooper LF. Early molecular assessment of osseointegration in humans. *Clin Oral Implants Res*. 2014;25(11): 1273-1285.
42. Kawanami A, Matsushita T, Chan YY, Murakami S. Mice expressing GFP and CreER in osteochondro progenitor cells in the periosteum. *Biochem Biophys Res Commun*. 2009;386(3):477-482.
43. Mendonça G, Mendonça DB, Simões LG, et al. Nanostructured alumina-coated implant surface: effect on osteoblast-related gene expression and bone-to-implant contact in vivo. *Int J Oral Maxillofac Implants*. 2009;24(2):205-215.
44. Mendonça G, Mendonça DBS, Simões LGP, et al. The effects of implant surface nanoscale features on osteoblast-specific gene expression. *Biomaterials*. 2009;30(25):4053-4062.

How to cite this article: Morandini Rodrigues L, Lima Zutin EA, Sartori EM, et al. Nanoscale hybrid implant surfaces and Osterix-mediated osseointegration. *J Biomed Mater Res*. 2022;110(3):696-707. doi:10.1002/jbm.a.37323